High-energy pulse synthesis with sub-cycle waveform control for strong-field physics

Shu-Wei Huang[1], Giovanni Cirmi[1], Jeffrey Moses[1], Kyung-Han Hong[1], Siddharth Bhardwaj[1], Jonathan R. Birge[1], Li-Jin Chen[1], Enbang Li[2], Benjamin J. Eggleton[2], Giulio Cerullo[3], and Franz X. Kärtner[1,4*]

[1]Department of Electrical Engineering and Computer Science and Research Laboratory of Electronics, Massachusetts Institute of Technology, Cambridge, Massachusetts 02139, USA

[2]Centre for Ultrahigh Bandwidth Devices for Optical Systems, Australian Research Council Centre of Excellence, School of Physics, University of Sydney, NSW 2006, Australia

[3]IFN-CNR, Dipartimento di Fisica, Politecnico di Milano, Piazza L. Da Vinci 32, 20133 Milano, Italy

[4]DESY-Center for Free-Electron Laser Science and Hamburg University, Notkestraße 85, D-22607 Hamburg, Germany

Over the last decade, control of atomic-scale electronic motion by non-perturbative optical fields has broken tremendous new ground with the advent of phase-controlled high-energy few-cycle pulse sources[1]. The development of close-to-single-cycle, carrier-envelope phase (CEP) controlled, high-energy optical pulses has already led to isolated attosecond EUV pulse generation[2], expanding ultrafast spectroscopy to attosecond resolution[1]. However, further investigation and control of these physical processes requires sub-cycle waveform shaping, which until now could not be achieved. Here we present a light source, utilizing coherent wavelength multiplexing, that enables sub-cycle waveform shaping with a two-octave-spanning spectrum and 15-μJ pulse energy. It

offers full phase control and allows generation of any optical waveform supported by the amplified spectrum. Both energy and bandwidth scale linearly with the number of sub-modules, thus the peak-power scales quadratically. The demonstrated system is the prototype of a class of novel optical tools for attosecond control of strong-field physics experiments.

Since the invention of pulsed lasers, the ultrafast laser science community has strived for ever broader optical bandwidths, shorter pulse durations, higher pulse energies, and improved phase control. Each breakthrough in the generation methods has led to new scientific discoveries, in a wide range of fields[3-5]. Recent investigations of phenomena at the intersection of ultrafast and strong-field laser physics, such as high-harmonic generation (HHG)[6] and strong-field ionization[7], has demanded that laser sources combine each of the breakthroughs mentioned above. Investigation and control of strong-field light-matter interaction simultaneously requires a multi-octave-spanning bandwidth, an isolated sub-cycle waveform, a peak-intensity above 10^{14} W/cm^2 and a full phase control. Such features would allow arbitrary shaping of the strong electric-field waveform for steering ionized electron wavepackets[8] and precise control of tunneling and multiphoton ionization events.

For over two decades, laser scientists have sought to extend laser bandwidths and achieve sub-cycle optical waveforms by synthesizing multiple laser sources[9]. Attempts to combine two independent mode-locked lasers have seen some success, *e.g.*, for frequency metrology[10, 11], but are challenging because of the differential phase noise

beyond the achievable feedback loop bandwidth. This problem was recently circumvented by coherently adding two pulse trains derived from the same fiber laser, resulting in the first demonstration of an isolated single-cycle optical pulse source[12]. This proved the feasibility of pulse synthesis at the nanojoule level, but achieving high pulse-energy requires synthesis of low-repetition-rate pulses, which is a challenge because of the environmental perturbations typical of high-energy amplifiers. An approach to high-energy pulse synthesis based on combining the pump, signal, and idler of a multi-cycle optical parametric amplifier is being investigated and it shows the potential to produce multiple single-cycle pulses under a multi-cycle envelope with pulse separation on the order of a few femtoseconds[13].

In this paper, we address the challenge of high-energy sub-cycle optical waveform synthesis. We demonstrate a new approach, based on coherent wavelength multiplexing of ultra-broadband optical parametric chirped pulse amplifiers (OPCPAs), for the generation of fully controlled high-energy non-sinusoidal optical waveforms with spectra spanning close to two octaves. By simulation, we present an example of the unique features of our source as a driver for isolated strong-field physics experiments: the confinement of the strong-field light-matter interaction to within an optical cycle and attosecond control of the interaction. The system coherently combines two CEP-controlled, few-cycle pulses obtained from different OPCPAs: 1) a near infrared (NIR)-OPCPA, producing 25-μJ, 9-fs pulses centered at 870 nm; and 2) a short-wavelength infrared (SWIR)-OPCPA, producing 25-μJ, 24-fs pulses centered at 2.15 μm. The ultra-broadband OPCPA is the most promising technology for producing wavelength-tunable,

high-peak-power and high-average-power, few-cycle optical pulses with good pre-pulse contrast[14]. Furthermore, an ultra-broadband OPCPA maintains good CEP stability due to the low thermal load and the small dispersion required to stretch and compress the signals.

Figure 1 shows a schematic of the system. It starts with an actively CEP-stabilized octave-spanning Ti:sapphire oscillator. Using a single oscillator as front-end for the entire system ensures the coherence of the two OPCPA pulses to within environmental fluctuations and drifts on subsequent beam paths. The designs of the OPCPAs follow the guidelines described in previous studies[15, 16] for simultaneously optimizing energy conversion, amplification bandwidth, and signal-to-noise ratio. Of note, the inclusion of an acousto-optic programmable dispersive filter (AOPDF) in each OPCPA allows independent spectral phase and amplitude adjustment of each pulse, enabling control and optimization of the synthesized waveform.

Outputs from the two OPCPAs are combined in a broadband neutral beamsplitter. The overall spectrum spans over 1.8 octaves (green lines in Fig. 2a) and the energy of the synthesized pulse is 15 μJ. Besides the spectral phases (controlled by the AOPDFs), three other independent parameters (see Fig. 1) determine the synthesized electric-field waveform: the CEP of the NIR-OPCPA pulse (ϕ_1), the CEP of the SWIR-OPCPA pulse (ϕ_2), and the relative timing between the two OPCPA pulses (Δt). Precise stabilization of these three parameters is required for coherent synthesis of the two OPCPA pulses, and subsequent control of each parameter allows precise waveform shaping. While the CEP of the SWIR-OPCPA is passively stabilized due to the intrapulse difference-frequency generation (DFG)[17] used to produce its seed, an active feedback loop on the oscillator is

implemented to ensure the CEP stability of the NIR-OPCPA. Figures 2d and 2e demonstrate the CEP stability of the two individual pulses, with r.m.s. fluctuations as low as 135 mrad and 127 mrad, respectively. Figure 2h characterizes the relative timing stability. A feedback loop based on a balanced cross-correlator (BCC) [18] is implemented to synchronize the two pulses, allowing attosecond-precision relative timing stability. With the feedback control of the SWIR-OPCPA's path length over a bandwidth of 30 Hz, the relative timing drift is reduced to 250 as, less than 5% of the oscillation period of the SWIR-OPCPA (7.2 fs).

Once the BCC-assisted feedback loop stabilizes the relative timing between the two OPCPA pulses, a two-dimensional spectral-shearing interferometer (2DSI)[19] is used to measure the frequency-dependent group-delay of the synthesized pulse. Figures 2b and 2c show the raw data of a 2DSI measurement while Fig. 2a plots (black lines) the extracted frequency-dependent group-delay of the synthesized pulse, which is the derivative of the spectral phase with respect to frequency. The 2DSI measurement shows that the two OPCPA pulses are temporally overlapped and each is well compressed to within 10% of its transform-limited pulse duration.

In our system, the CEPs can be varied by slight tuning of any dispersive element, including the AOPDFs[20]. The values of the CEP will be determined automatically *in situ* when strong-field experiments are conducted[21] and hence CEP tunability is sufficient from an experimental point-of-view. In summary, our system is capable of stabilizing and controlling all independent parameters that define the synthesized electric-field waveform. Figure 3a plots a synthesized electric-field waveform and intensity profile

assuming the CEPs (ϕ_1=650mrad, ϕ_2=-750mrad) optimal for achieving the shortest high-field transient, which lasts only 0.8 cycles (amplitude FWHM) of the carrier (centroid) frequency (λ_c = 1.26 μm). The lower inset of Fig. 3a clearly shows that the synthesized electric-field waveform is non-sinusoidal and the main feature lasts less than an optical cycle. As an example of waveform shaping made possible by tuning parameters of our system, Fig. 3b and 3c show two atypical waveforms as the CEP and the relative timing are changed. Due to the large gap in the combined spectrum, there are wings 4.8 fs from the central peak as shown in Fig. 3a. As we will show below, for processes initiated by strong-field ionization, these wings have a negligible effect. For more demanding applications, the wings can be suppressed by extension of the coherent wavelength multiplexing scheme to include a third OPCPA, centered at 1.5 μm[22], to fill the spectral gap. The synthesized waveforms are important for optimizing the HHG process[6], which is to date the only demonstrated technique for generating isolated attosecond pulses[2]. As an example, we numerically solve the time-dependent Schrödinger equation (TDSE) for a He-atom in a strong laser field to illustrate a possible use of our source for driving direct isolated soft-x-ray pulse generation (Fig. 4). The achievable peak intensity ($6x10^{14}$ W/cm^2) is chosen such that the total ionization is below the critical ionization level in helium[23]. With choice of CEPs as in Fig. 4a, substantial ionization is limited to one optical half-cycle and an isolated soft-x-ray pulse spanning over 250 eV is generated (Fig. 4b and 4c) without the need for gating techniques[24] or spectral filtering which typically limit the obtainable bandwidth. Using an additional Sn filter, which blocks the strong IR driving field and the nonlinearly chirped low-photon-energy spectral content

below 70 eV, leads to an isolated 150-as pulse centered at 200 eV. Of note, the non-sinusoidal electric-field waveform leads to drastically changed electron trajectories (compared to those from a sinusoidal driving field) resulting in corresponding changes in quantum diffusion and atto-chirp, which can be controlled by means of the waveform synthesis parameters (ϕ_1, ϕ_2, and Δt). In this example, quantum diffusion dominates over ionization rate (see Supplementary Information) and effectively eliminates the radiation from long trajectories, resulting in isolated soft-x-ray pulse generation solely from short trajectories (Fig. 4b). This gives an example of the capability of our light source to simultaneously isolate the ionization process and manipulate electron trajectories within an optical cycle, allowing unprecedented control of the HHG process.

In conclusion, we have presented a scalable waveform synthesis scheme based on fully controlled coherent wavelength multiplexing of high-energy, few-cycle optical pulses from multi-color OPCPAs. Currently, the system generates a non-sinusoidal waveform that can be used to drive an isolated strong-field physics experiments. The pulse energy is 15-μJ with the spectrum spanning close to two octaves, and it can be readily scaled both in energy and bandwidth given the proven wavelength tunability of OPCPAs[25] (see Supplementary Information). A numerical study shows the uniqueness of our source for direct isolated soft-x-ray pulse generation based on HHG, eliminating the need for gating techniques[24] or spectral filtering. In addition to this application, this new high-intensity laser architecture can be applied to optical field-emission[26], tunneling ionization studies[27], time-resolved spectroscopy[28], and in general, attosecond control of strong-field physics experiments.

Methods:

OPCPA setup:

Supplementary Fig. S1 shows the system schematic. Both OPCPAs are pumped by an optically synchronized (injection seeded by the Octavius-85M Ti:sapphire oscillator from IdestaQE, Inc.) Nd:YLF chirped pulse amplifier (CPA) which generates 3.5-mJ, 12-ps pulses at 1047 nm. The SWIR-OPCPA, pumped by 1 mJ of the Nd:YLF CPA output, follows the design method in ref. 15. The seed, produced by intrapulse DFG of the oscillator, is first stretched by a bulk silicon block to 5 ps and pre-amplified to 1.5 μJ in the first OPCPA stage using periodically poled lithium niobate (PPLN). The pre-amplified pulse is further stretched to 9.5 ps by an infrared AOPDF, amplified to 25 μJ in periodically poled stoichiometric lithium tantalate (PPSLT), and then compressed to 9 fs in a broadband anti-reflection coated quartz glass block (Suprasil 300). For the NIR-OPCPA, a 2-mJ fraction of the Nd:YLF CPA output is frequency doubled in a lithium triborate (LBO) crystal and used to amplify the oscillator output. The seed is first stretched to 5 ps by a Brewster prism stretcher. The signal is pre-amplified in a double-pass configuration in a type-I, 5-mm-long β-barium borate (BBO) crystal to 2 μJ. The amplified pulse is further stretched to 6.2 ps by an AOPDF and a grating stretcher, amplified to 25 μJ in BBO and then compressed to 24 fs in a Brewster-cut N-LaSF9 block.

Beam combining:

The outputs of the two OPCPAs are combined in a broadband neutral beamsplitter,

which introduces 25% energy loss. In addition, only half of the synthesized pulse energy is available for an experiment because the other half is directed to the balanced cross-correlator (BCC). Since the pulse energy directed to the BCC is much more than is needed, a custom-made dichroic mirror can be implemented to improve the experimentally available pulse energy by a factor of 2.5. Thus in an optimized system, the waveform synthesis could be achieved with very low losses.

We choose to combine the two OPCPA pulses in a "constant waist width" fashion[29], which is inherently compatible with OPCPA configurations. As shown theoretically in ref. 29, the "constant waist width" configuration offers the unique property that the temporal pulse form remains unchanged upon propagation.

Relative timing stabilization:

One part of the combined beam is directed to a BCC (Supplementary Fig. S2) which consists of two nearly identical cross-correlators using 200-μm-thick BBO crystals, phase matched for sum-frequency generation of 870-nm light and 2.15-μm light. Use of the SWIR-OPCPA delay stage and a 4-mm-thick calcium fluoride (CaF2) window between cross-correlators sets the group delay between pulses to +25 fs in one cross-correlator and -25 fs in the other. An additional 2-mm-thick calcium fluoride window ensures zero group delay ($\Delta t = 0.0$ fs) at the combined output. For deviations from this zero-delay configuration of up to ±20 fs, the photodetector signal is linearly proportional to the time difference and thus can be used as the error signal fed to the loop filter in the feedback system. Furthermore, in the vicinity of the zero crossing, the setup delivers a balanced

signal and thus the amplitude noise of each OPCPA output does not affect the detected error signal.

2DSI:

In the 2DSI setup (Supplementary Fig. S3), the combined beam is first split by a beam sampler whose second surface is anti-reflection coated. A copy of the beam (4%) is Fresnel reflected and only guided via silver mirrors before being mixed in a 40-μm type II BBO. The other copy of the beam (96%) passes through the beam sampler and is highly stretched before being equally split again by a cube beamsplitter, routed to the BBO and mixed with the unchirped pulse. Two collinear, temporally overlapped, but spectrally sheared upconverted pulses are then generated. To observe the interference between the two upconverted pulses, which encodes the spectral group delay information, the delay of one of the highly chirped pulses is scanned over a few optical cycles. The spectrum of the upconverted signal is recorded as a function of this delay, yielding a two-dimensional intensity function that is shown in Fig. 2b and 2c. The interpretation of the 2DSI data is relatively straight-forward: each spectral component is vertically shifted in proportion to its group delay.

It should be noted that we treat the combined beam as a single pulse here and use the 2DSI to retrieve the frequency-dependent group delay of the synthesized pulse, and not just those of the individual OPCPA pulses. That is, we measured the combined beam, not the two OPCPA pulses independently, and the portion mixed with the unchirped pulse is purely derived from the NIR-OPCPA such that the measured spectral group

delay has a definite reference throughout the whole spectrum from 700nm to 2500nm. A different relative timing results in a vertical shift of the fringe patterns in Fig. 2b and 2c.

References:

1. Krausz, F. & Ivanov, M. Attosecond physics. *Rev. Mod. Phys.* **81**, 163-234 (2009).
2. Goulielmakis, E. *et al.* Single-cycle nonlinear optics. *Science* **320**, 1614-1617 (2008).
3. Udem, T., Holzwarth, R. & Hänsch, T.W. Optical frequency metrology. *Nature* **416**, 233-237 (2002).
4. Kienberger, R. *et al.* Atomic transient recorder. *Nature* **427**, 817-821 (2004).
5. Li, C.H. *et al.* A laser frequency comb that enables radial velocity measurements with a precision of 1 cm s(-1). *Nature* **452**, 610-612 (2008).
6. Corkum, P.B. Plasma perspective on strong field multiphoton ionization. *Phys. Rev. Lett.* **71**, 1994-1997 (1993).
7. Keldysh, L.V. Ionization in the field of a strong electromagnetic wave. *Soviet Physics JETP* **20**, 1307-1314 (1965).
8. Chipperfield, L.E., Robinson, J.S., Tisch, J.W.G. & Marangos, J.P. Ideal waveform to generate the maximum possible electron recollision energy for any given oscillation period. *Phys. Rev. Lett.* **102**, 063003 (2009).
9. Hänsch, T.W. A proposed sub-femtosecond pulse synthesizer using separate phase-locked laser oscillators. *Opt. Commun.* **80**, 71-75 (1990).

10. Wei, Z.Y., Kobayashi, Y., Zhang, Z.G. & Torizuka, K. Generation of two-color femtosecond pulses by self-synchronizing Ti : sapphire and Cr : forsterite lasers. *Opt. Lett.* **26**, 1806-1808 (2001).
11. Shelton, R.K. *et al.* Phase-coherent optical pulse synthesis from separate femtosecond lasers. *Science* **293**, 1286-1289 (2001).
12. Krauss, G. *et al.* Synthesis of a single cycle of light with compact erbium-doped fibre technology. *Nature Photon.* **4**, 33-36 (2010).
13. Cerullo, G., Baltuška, A., Mücke, O.D. & Vozzi, C. Few-optical-cycle light pulses with passive carrier-envelope phase stabilization. *Laser & Photon. Rev.* **5**, 323 (2011).
14. Dubietis, A., Butkus, R. & Piskarskas, A.P. Trends in chirped pulse optical parametric amplification. *IEEE J. Sel. Top. Quant.* **12**, 163-172 (2006).
15. Moses, J. *et al.* Highly stable ultrabroadband mid-IR optical parametric chirped-pulse amplifier optimized for superfluorescence suppression. *Opt. Lett.* **34**, 1639-1641 (2009).
16. Moses, J., Manzoni, C., Huang, S.W., Cerullo, G. & Kärtner, F.X. Temporal optimization of ultrabroadband high-energy OPCPA. *Opt. Express* **17**, 5540-5555 (2009).
17. Baltuška, A., Fuji, T. & Kobayashi, T. Controlling the carrier-envelope phase of ultrashort light pulses with optical parametric amplifiers. *Phys. Rev. Lett.* **88**, 1339011 (2002).
18. Schibli, T.R. *et al.* Attosecond active synchronization of passively mode-locked lasers by balanced cross correlation. *Opt. Lett.* **28**, 947-949 (2003).

19. Birge, J.R., Crespo, H.M. & Kärtner, F.X. Theory and design of two-dimensional spectral shearing interferometry for few-cycle pulse measurement. *J. Opt. Soc. Am. B* **27**, 1165-1173 (2010).

20. Forget, N., Canova, L., Chen, X., Jullien, A. & Lopez-Martens, R. Closed-loop carrier-envelope phase stabilization with an acousto-optic programmable dispersive filter. *Opt. Lett.* **34**, 3647-3649 (2009).

21. Wittmann, T. *et al.* Single-shot carrier-envelope phase measurement of few-cycle laser pulses. *Nature Phys.* **5**, 357-362 (2009).

22. Mücke, O.D. *et al.* Scalable Yb-MOPA-driven carrier-envelope phase-stable few-cycle parametric amplifier at 1.5 μm. *Opt. Lett.* **34**, 118-120 (2009).

23. Popmintchev, T. *et al.* Phase matching of high harmonic generation in the soft and hard X-ray regions of the spectrum. *Proc. Natl. Acad. Sci. USA* **106**, 10516-10521 (2009).

24. Sansone, G. *et al.* Isolated Single-Cycle Attosecond Pulses. *Science* **314**, 443-446 (2006).

25. Cerullo, G. & De Silvestri, S. Ultrafast optical parametric amplifiers. *Rev. Sci. Instrum.* **74**, 1-18 (2003).

26. Hommelhoff, P., Kealhofer, C. & Kasevich, M.A. Ultrafast electron pulses from a tungsten tip triggered by low-power femtosecond laser pulses. *Phys. Rev. Lett.* **97**, 247402 (2006).

27. Arissian, L. *et al.* Direct Test of Laser Tunneling with Electron Momentum Imaging. *Phys. Rev. Lett.* **105**, 133002 (2010).

28. Hochstrasser, R.M. Two-dimensional spectroscopy at infrared and optical frequencies. *Proc. Natl. Acad. Sci. USA* **104**, 14190-14196 (2007).

29. Zou, Q.H. & Lu, B. Propagation properties of ultrashort pulsed beams with constant waist width in free space. *Opt. Laser Technol.* **39**, 619-625 (2007).

Acknowledgement:

This work was supported by Air Force Office of Scientific Research grants FA9550-09-1-0212, FA8655-09-1-3101 and FA9550-10-1-0063 and by Progetto Roberto Rocca.

Materials & Correspondence:

Franz X. Kärtner is the corresponding author.

Author contributions:

FXK, KHH, JM, and SWH conceived the experiment, and together with GC and GC carried it out; SB provided the TDSE simulation and the spectrogram analysis; JRB provided critical discussion on 2DSI; LJC provided critical help and discussion on the Ti:sapphire oscillator; EL and BJE provided the chirped fiber Bragg grating; FXK, GC, KHH, JM, GC, and SWH co-wrote the paper. FXK is the senior author from the group and supervised the work.

Figure captions:

Figure 1
Scheme of the high-energy optical waveform synthesizer. Two CEP-stabilized, few-cycle OPCPAs centered at different wavelengths are combined based on the concept of coherent wavelength multiplexing to produce a fully controlled non-sinusoidal optical waveform with 15-μJ pulse energy at 1-kHz repetition rate. Full control over the optical phase allows for any optical waveform given the amplified spectrum. YDFA: Ytterbium-doped fiber amplifier; BPF: bandpass filter.

Figure 2
Characterization of the synthesized pulses. (a) The optical spectrum and the frequency-dependent group-delay of the synthesized pulses. The overall spectrum spans over 1.8 octaves and supports non-sinusoidal waveforms with sub-cycle features. (b) is the 2DSI trace for the NIR-OPCPA and (c) is that for the SWIR-OPCPA. The 2DSI measurement shows that the two pulses are temporally overlapped and well compressed to within 10% of the transform-limited pulse duration. CEP stabilities are verified using nonlinear interferograms with 5-shot integration. (d) f-2f interferogram, measuring 135 mrad rms CEP fluctuations over 30 s for the NIR-OPCPA. (e) f-3f interferogram, measuring 127 mrad rms CEP fluctuations over 30 s for the SWIR-OPCPA. Spatial properties are characterized by measuring the beam profiles and the M^2-values. (f) shows a beam profile of the NIR-OPCPA and (g) shows that of the SWIR-OPCPA. The M^2-value of the NIR-OPCPA is 1.2 and that of the SWIR-OPCPA is 1.3. The BCC-assisted feedback loop guarantees the relative timing stability and (h) shows BCC measurements of the free-running system (black) and the closed-loop system (red). The closed-loop system ensures a relative timing drift of 250 as, less than 5% of the oscillation period of the SWIR-OPCPA, over 10 s.

Figure 3
The synthesized electric-field waveforms. (a) Here we assume CEPs (ϕ_1=650 mrad, ϕ_2=-750 mrad) optimal for achieving the shortest high-field transient, which lasts only 0.8 cycles (amplitude FWHM) of the carrier (centroid) frequency. Lower inset: the waveform is plotted in a shorter time window and superimposed with the electric field oscillating at the carrier (centroid) frequency, showing that the synthesized electric-field waveform is non-sinusoidal and the main feature lasts less than an optical cycle. Upper inset: corresponding intensity profile. About one third of the pulse energy is contained in the main pulse. As an example of waveform shaping made possible by tuning parameters of our system, two additional atypical waveforms are shown. (b) A synthesized waveform by adding 500 mrad to both ϕ_1 and ϕ_2. (c) A synthesized waveform by adding 1 fs to Δt.

Figure 4
Extreme nonlinear optics with sub-cycle manipulated waveforms. TDSE simulation results of the single-atom HHG show the uniqueness of our source for direct isolated soft x-ray pulse generation. (a) Ionization dynamics (red) induced in helium by a linearly polarized electric-field waveform (black) assuming a peak intensity of 6×10^{14} W/cm^2, ϕ_1=960 mrad, and ϕ_2=-440 mrad. (b) Spectrogram of the HHG superimposed with the

calculated classical trajectories. Returning trajectories from three ionization events (2: the main pulse; 1 and 3: the satellite pulses) are shown for clear interpretation of the spectrogram. The synthesized pulse isolates the ionization process to a half optical cycle and a continuum spectrum spanning more than 250eV can be achieved. The isolated soft x-ray pulse has the same sign of chirp over 80% of the spectrum and so the compression setup can be simplified. (c) The isolated soft x-ray pulse plotted in the time domain before (pink) and after (black line) a 100-nm thick Sn filter. The Sn filter is chosen for its capability to block the strong IR driving field and the nonlinearly chirped low-photon-energy spectral content, and its good transmission in the soft x-ray range. The filtered isolated soft x-ray pulse has a FWHM duration of 150 as.

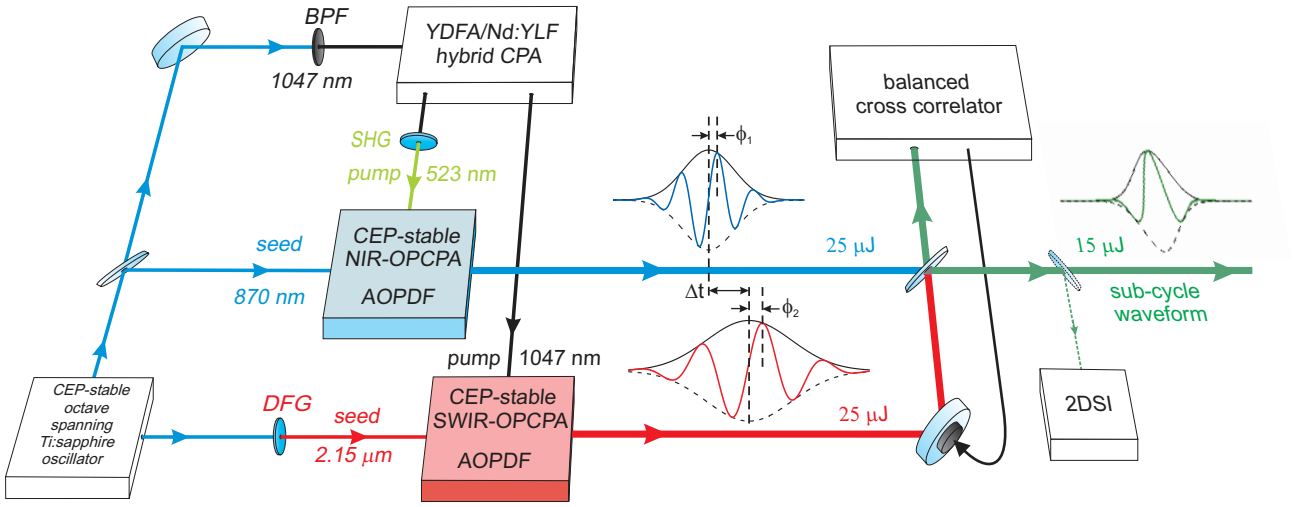
BPF
1047 nm
YDFA/Nd:YLF
hybrid CPA
SHG
pump
523 nm
seed
870 nm
CEP-stable
NIR-OPCPA
AOPDF
pump
1047 nm
CEP-stable
octave
spanning
Ti:sapphire
oscillator
DFG
seed
2.15 μm
CEP-stable
SWIR-OPCPA
AOPDF
balanced
cross correlator
25 μJ
25 μJ
15 μJ
sub-cycle
waveform
2DSI
Δt

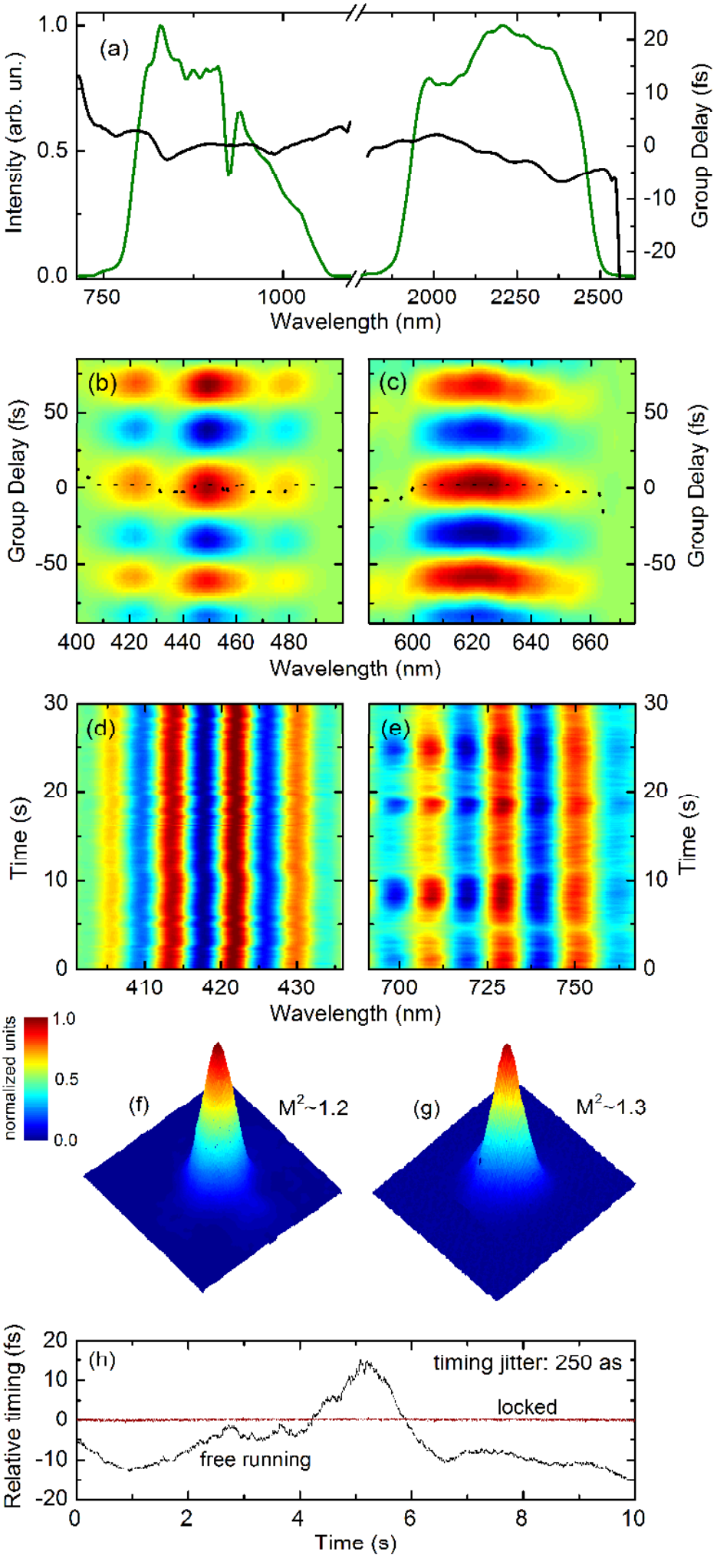
(a)
Intensity (arb. un.)
Group Delay (fs)
Wavelength (nm)
(b)
(c)
Group Delay (fs)
Wavelength (nm)
(d)
(e)
Time (s)
Wavelength (nm)
normalized units
(f)
M²~1.2
(g)
M²~1.3
(h)
timing jitter: 250 as
locked
free running
Relative timing (fs)
Time (s)

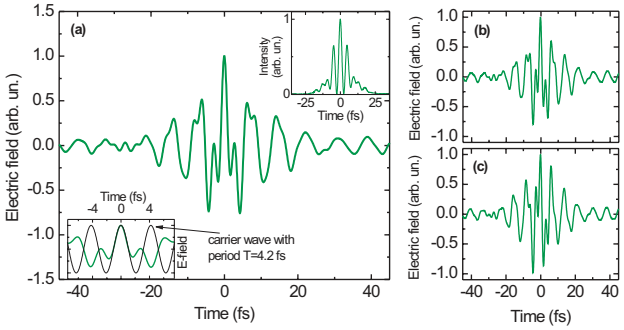
(a)
(b)
(c)
Electric field (arb. un.)
Time (fs)
Intensity (arb. un.)
E-field
carrier wave with
period T=4.2 fs

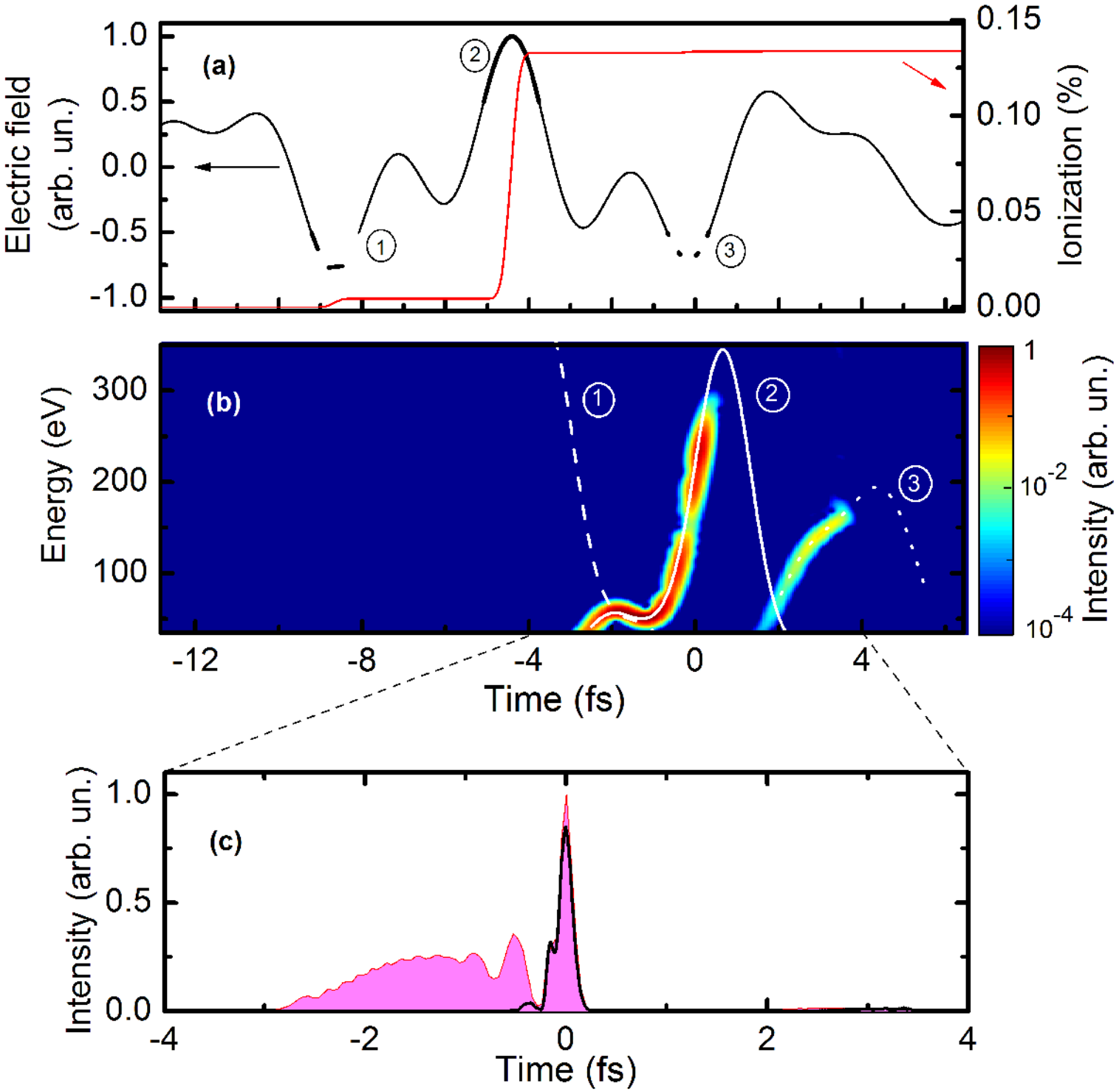
(a)
Electric field (arb. un.)
1.0
0.5
0.0
-0.5
-1.0
Ionization (%)
0.15
0.10
0.05
0.00
①
②
③
(b)
Energy (eV)
300
200
100
-12
-8
-4
0
4
Time (fs)
1
10^{-2}
10^{-4}
Intensity (arb. un.)
(c)
Intensity (arb. un.)
1.0
0.5
0.0
-4
-2
0
2
4
Time (fs)

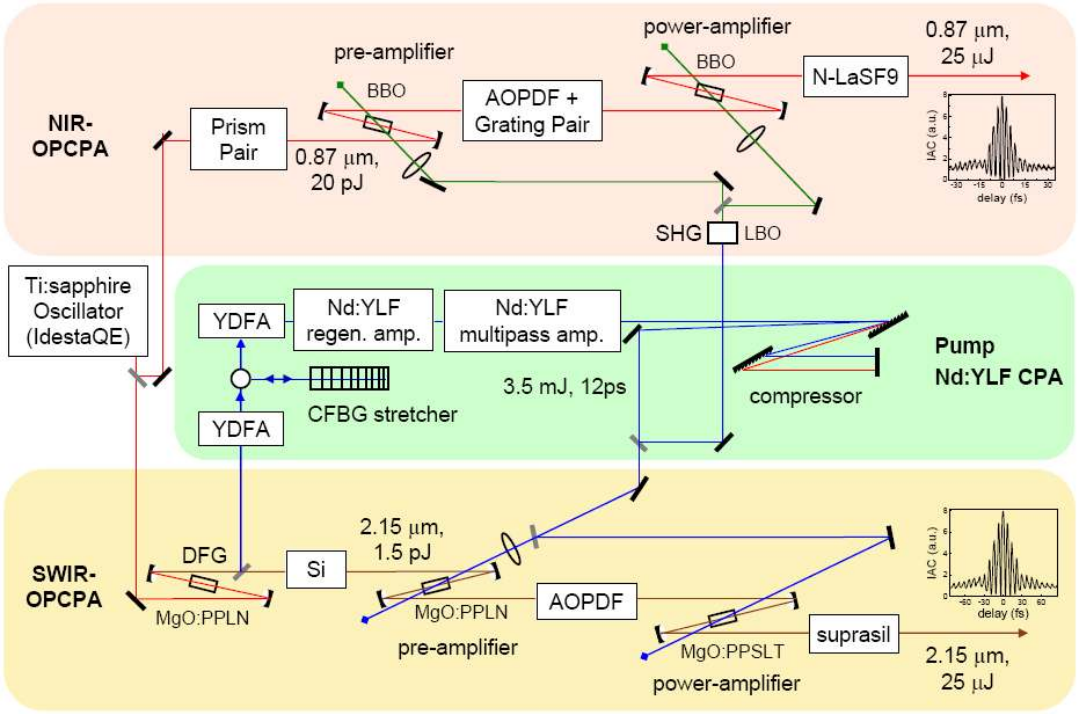

Figure S1. Schematics of the Nd:YLF CPA pump, the NIR-OPCPA, and the SWIR-OPCPA. YDFA: Ytterbium-doped fiber amplifier; CFBG: chirped fiber Bragg grating; AOPDF: acousto-optic programmable dispersive filter.

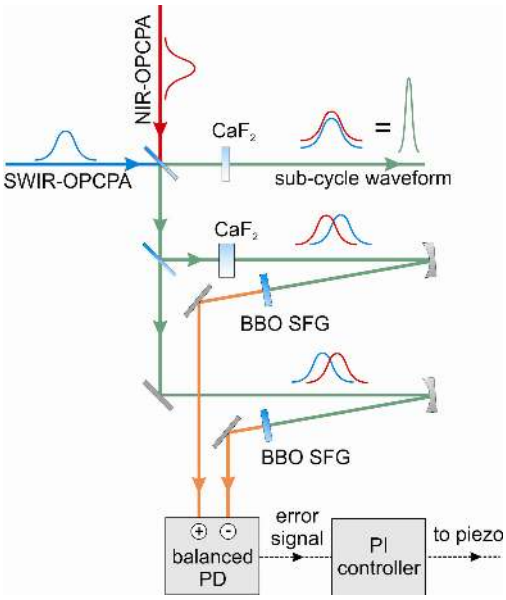

Figure S2. Schematics of the balanced cross-correlator.

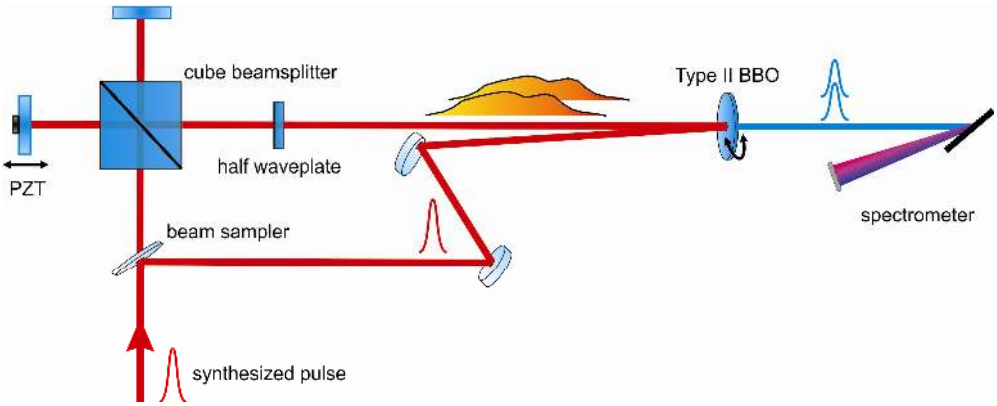

Figure S3. Schematics of the two-dimensional spectral-shearing interferometer.

Effect of jitters:

As described in the paper, we stabilize three important parameters: the CEP of the NIR-OPCPA (ϕ_1), the CEP of the SWIR-OPCPA (ϕ_2), and the relative timing between the two OPCPAs (Δt). Since these parameters significantly influence the synthesized electric-field waveform, it is important to make sure the residual jitters are sufficiently small to impart only a negligible effect. Figure S4 shows the synthesized electric-field waveforms under the r.m.s. residual jitters (black dotted line) superimposed with the unperturbed waveform (red solid line). To quantify the waveform difference, we calculate the relative squared error (RSE) in a 10-fs time window which covers the main pulse as well as the two satellite pulses. Currently the 250-as relative timing jitter results in the largest waveform change (2.22% RSE), but it can be further reduced with a broader feedback bandwidth.

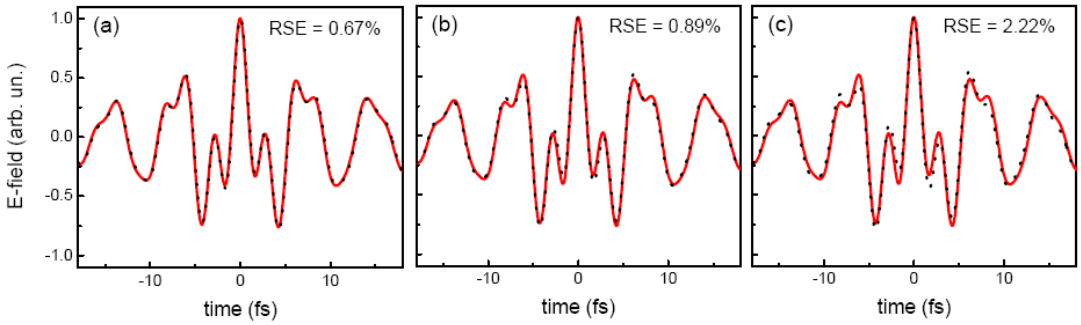

Figure S4. Waveforms under r.m.s. residual jitters. While the red solid line is the unperturbed waveform as shown in Fig. 3, the black dotted line is obtained by adding 135 mrad to ϕ_1 in (a), adding 127 mrad to ϕ_2 in (b), and adding 250 as to Δt in (c).

In principle, one can choose another way to stabilize these three parameters: first stabilize the CEP of one of the OPCPA pulses (ϕ_1), then stabilize the relative phase between the two OPCPA pulses ($\Delta\phi$), and finally stabilize the relative timing between the two OPCPA pulses (Δt). Since the measurement of $\Delta\phi$ will inevitably be influenced by the change in Δt, diagonalization of the effects from $\Delta\phi$ and Δt becomes critically important and any error in determining the transfer function will lead to residual jitters. In contrast, our method inherently diagonalizes all three parameters so that we can achieve lower residual jitters. In addition, there is only one relative measurement necessary in our method, which thus provides greater scalability and flexibility in the context of modular design.

Scaled-up system and tuning of the pulse synthesis parameters:

The concept and technology demonstrated here can be further scaled in both energy and bandwidth to expand its applicability to strong-field physics experiments. The pulse energy of each individual OPCPA is ready to be scaled to the multi-mJ level at kHz repetition rates using picosecond cryogenically-cooled Yb:YAG pump lasers[1], providing high average-power, currently at the 100-W level. Besides, since the feedback loop used

for relative timing stabilization requires only a 30-Hz bandwidth, the system can be immediately scaled up to higher pulse energy at even lower repetition rate.

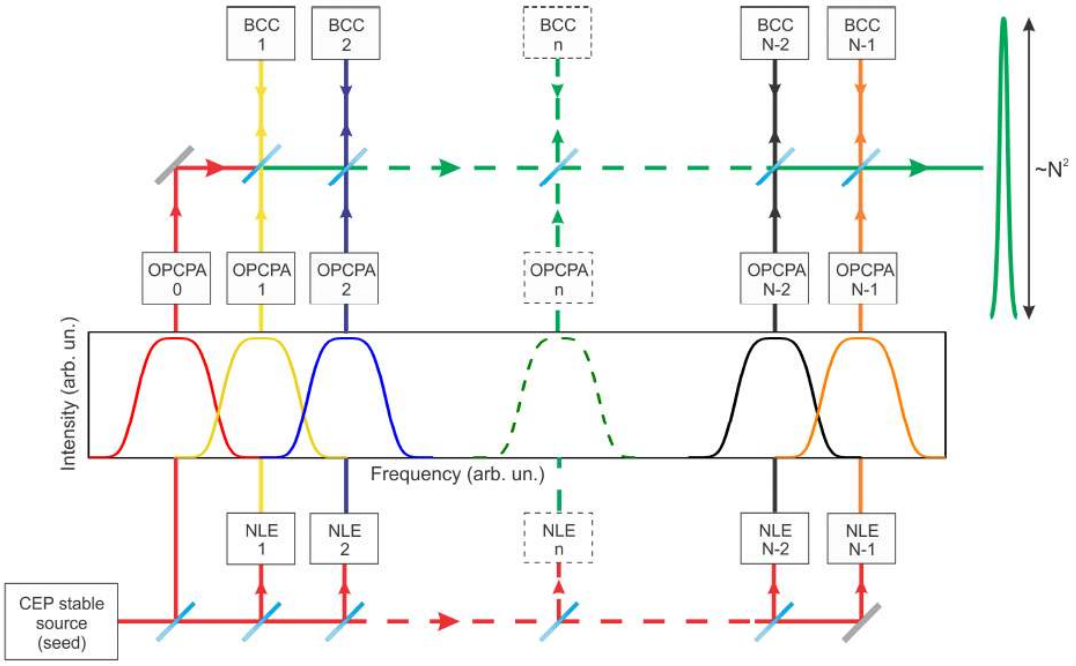

Figure S5. Schematics of the proposed scaled-up system.

Figure S5 shows a schematic of the proposed scaled-up system. It is comprised of a number of OPCPAs seeded by a single CEP-stabilized light source both directly and through nonlinear effects (NLEs) which preserve the CEP stability such as intrapulse DFG, self-phase modulation, and Raman shifting. The OPCPA pulses are combined in custom-made dichroic mirrors and the BCC-assisted feedback loops stabilize the relative timing. The simple coherent beam combination of identical optical amplifiers leads to a peak-power that scales linearly with the number of sub-modules N. In the proposed system, the wavelength multiplexing capability provided by the OPCPAs improves the synthesized pulse peak-power by another factor of N, through scaling of the total bandwidth. Overall, the system, which implements coherent addition by wavelength multiplexing, boosts the peak power favorably by N^2.

The wavelength multiplexing gives us additional flexibility to control and optimize the synthesized waveform because each individual OPCPA has to amplify only a moderate bandwidth, much less than an octave. In this regime, the CEP (relative to the reference module) and the relative timing can be approximately lumped as only one independent variable. For a system consisting of N sub-modules, only N feedback loops are necessary as opposed to 2N-1. Figure S6 depicts the concept using the 3-cycle pulses described in this paper. Assume now we shift the CEP of the SWIR-OPCPA pulses by π compared to the condition which results in the synthesized waveform shown in Fig. 3a (red solid line here). The effect of the CEP shift on the synthesized waveform can be

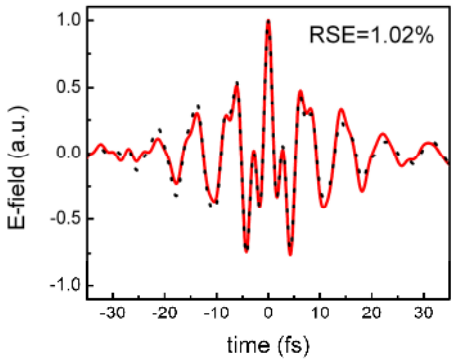

Figure S6. While the red solid line is the unperturbed waveform as shown in Fig. 3a, the black dotted line is obtained by adding a CEP shift of π and a relative timing of 3.6 fs to the SWIR-OPCPA pulses. The waveform difference is comparable to a CEP jitter of 100 mrad.

cancelled by changing the relative timing by 3.6 fs (black dotted line). The waveform difference in a window of 26 fs, which contains 86% of the pulse energy, is only 1.02% (relative squared error). A CEP jitter of 100 mrad will result in the same relative squared error. Thus we conclude that control of the reference module's CEP and the relative timing is sufficient for systems based on synthesizing 3-cycle (or more) pulses.

HHG simulation:

The dipole approximation is used in describing the light-atom interaction both for the trajectory calculation and for solving the time-dependent Schrödinger equation (TDSE). Under the single-active electron approximation, the 3D TDSE is solved numerically with an asymptotic behavior correspondence discretization of the Hamiltonian[2]. The atomic potential of helium is modeled as described in ref. 3, and we optimize the coefficients for agreement between the calculated and measured ionization energies for helium. The dipole acceleration, and hence the HHG radiation, is then evaluated using the Ehrenfest theorem. The spectrogram (Fig. 4b) is calculated using a short-time Fourier transform with a Gaussian windowing function of 58 as (FWHM).

To gain more insights into the results given by the 3D TDSE simulation, we also calculated the ionization dynamics using ADK formula (the red curve in Fig. 4a) and the classical electron trajectories (overlaid on top of the spectrogram in Fig. 4b). Electron trajectories from three ionization events, which are labeled in numbers, are calculated and those trajectories that return to the ionized atom are shown in Fig. 4b. For visualization purpose, electrons ionized by the electric field with strength weaker than half of the maximum are neglected since they have negligible contribution to the HHG emission, as confirmed by the TDSE simulation.

In HHG, quantum diffusion and ionization rate are two competing factors in determining the ratio between radiation from long and short electron trajectories. While quantum diffusion always favors the short trajectories, when the HHG process is driven by conventional sinusoidal electric-field waveforms, stronger ionization rate for the long trajectories results in significant radiation from electrons of both trajectories. For the

example shown in Fig. 4b, where a sub-cycle waveform is used, the difference in travel time between long and short trajectories is increased. In addition, the ionization contribution to short trajectory radiation is boosted. Overall, quantum diffusion dominates and effectively eliminates the radiation from long trajectories, resulting in isolated soft x-ray pulse generation solely from short trajectories.

The peak intensity ($6x10^{14}$ W/cm^2) is chosen such that the total ionization is below the critical ionization level in helium. This intensity can be reached with a beam diameter of 27 μm ($1/e^2$). The transmission and dispersion of the Sn filter used for Fig. 4c are taken from ref. 4.

1. Hong, K.H. *et al.* High-energy, kHz-repetition-rate, ps cryogenic Yb:YAG chirped-pulse amplifier. *Optics Letters* **35**, 1752 (2010).
2. Gordon, A., Jirauschek, C. & Kärtner, F.X. Numerical solver of the time-dependent Schrodinger equation with Coulomb singularities. *Physical Review A* **73**, 042505 (2006).
3. Tong, X.M. & Lin, C.D. Empirical formula for static field ionization rates of atoms and molecules by lasers in the barrier-suppression regime. *Journal of Physics B-Atomic Molecular and Optical Physics* **38**, 2593 (2005).
4. Henke, B.L., Gullikson, E.M. & Davis, J.C. X-ray interactions: photoabsorption, scattering, transmission, and reflection at E=50-30000 eV, Z=1-92. *Atomic Data and Nuclear Data Tables* **54**, 181 (1993).